

HIGH RESOLUTION X-RAY IMAGING OF SUPERNOVA REMNANT 1987A

C.-Y. NG¹, B. M. GAENSLER¹, S. S. MURRAY², P. O. SLANE², S. PARK³, L. STAVELEY-SMITH⁴, R. N. MANCHESTER⁵,
D. N. BURROWS³

Accepted by ApJL

ABSTRACT

We report observations of the remnant of Supernova 1987A with the High Resolution Camera (HRC) onboard the *Chandra X-ray Observatory*. A direct image from the HRC resolves the annular structure of the X-ray remnant, confirming the morphology previously inferred by deconvolution of lower resolution data from the Advanced CCD Imaging Spectrometer. Detailed spatial modeling shows that the a thin ring plus a thin shell gives statistically the best description of the overall remnant structure, and suggests an outer radius $0.96'' \pm 0.05'' \pm 0.03''$ for the X-ray-emitting region, with the two uncertainties corresponding to the statistical and systematic errors, respectively. This is very similar to the radius determined by a similar modeling technique for the radio shell at a comparable epoch, in contrast to previous claims that the remnant is 10-15% smaller at X-rays than in the radio band. The HRC observations put a flux limit of 0.010 cts s^{-1} (99% confidence level, 0.08-10 keV range) on any compact source at the remnant center. Assuming the same foreground neutral hydrogen column density as towards the remnant, this allows us to rule out an unobscured neutron star with surface temperature $T^\infty > 2.5 \text{ MK}$ observed at infinity, a bright pulsar wind nebula or a magnetar.

Subject headings: circumstellar matter — shock waves — supernovae: individual (SN 1987A) — supernova remnants — X-rays: general — stars: neutron

1. INTRODUCTION

The core-collapse supernova (SN) 1987A in the Large Magellanic Cloud was the brightest SN observed since the invention of modern telescopes, providing the best opportunity to study the last evolutionary stage of a massive star. Optical observations have revealed a triple-ring nebula centered on the explosion, consisting of an inner equatorial ring of radius $0.81''$ - $0.86''$ and two larger outer rings (Burrows et al. 1995; Plait et al. 1995). These are part of the hourglass-shaped circumstellar medium (CSM) ejected by the progenitor 20,000 years ago (see Morris & Podsiadlowski 2007). Since early 2004, the SN blast wave has begun to encounter the main body of inner ring (Park et al. 2005, 2006). This ‘big crash’ has led to a drastic increase in soft X-ray emission that originates from the optically thin thermal plasma behind the shock. The X-ray spectrum is well-described by a two-component plane-parallel shock model in nonequilibrium ionization, with plasma temperatures $kT \sim 2$ and 0.3 keV , corresponding to the fast and decelerated shocks, respectively (Park et al. 2004, 2006). As the blast wave propagates into the dense CSM, the soft X-ray emission traces the evolution of the forward shock, probing the CSM structure and its density profile.

The nearness of SN 1987A (51.4 kpc) allows us to resolve a supernova remnant (SNR) morphology at a very

young age. In X-rays, this is only possible with the *Chandra X-ray Observatory*, the highest resolution X-ray telescope compared to any previous, current and even planned future X-ray missions. Previous *Chandra* observations of SNR 1987A were all carried out by the Advanced CCD Imaging Spectrometer (ACIS). However, the ACIS detector has a pixel size $0.492''$, comparable to the full width at half maximum (FWHM) of the mirror’s on-axis point-spread function (PSF). Although the effective resolution can be slightly improved by the dithering of the spacecraft and by applying a sub-pixel imaging algorithm (Tsunemi et al. 2001), image deconvolution is still required to fully resolve the remnant structure (e.g. Burrows et al. 2000). To determine whether artifacts are introduced by the complicated non-linear reconstruction process, the ACIS results need to be compared with higher resolution direct X-ray images. An analogy can be drawn from the radio imaging campaign of SNR 1987A. Since 1992, Australia Telescope Compact Array (ATCA) observations at 9 GHz have revealed detailed structure of the radio shell using the super-resolved technique, but it was not until the upgrade of the ATCA in 2003 that the higher resolution diffraction-limited images at 18 GHz provided a direct image of the radio morphology (see review by Gaensler et al. 2007).

The High Resolution Camera (HRC) onboard *Chandra*, consisting of two microchannel plate detectors, offers smaller electronic readout pixels ($0.13175''$) than ACIS. These better sample the PSF, providing a more straightforward imaging process without the need for deconvolution. Despite a smaller effective area for HRC than ACIS and the lack of any spectral resolution, the SNR is now very bright in X-rays below 2 keV, at which the HRC has good sensitivity, making it an ideal instrument for morphological studies. In this Letter, we report a detailed analysis of the first HRC observation of SNR 1987A.

Electronic address: ncy@physics.usyd.edu.au

¹ Sydney Institute for Astronomy, School of Physics, The University of Sydney, NSW 2006, Australia

² Harvard-Smithsonian Center for Astrophysics, Cambridge, MA 02138, USA

³ Department of Astronomy and Astrophysics, Pennsylvania State University, University Park, PA 16802, USA

⁴ International Centre for Radio Astronomy Research, School of Physics, The University of Western Australia, Crawley, WA 6009, Australia

⁵ Australia Telescope National Facility, CSIRO, Marsfield, NSW 1710, Australia

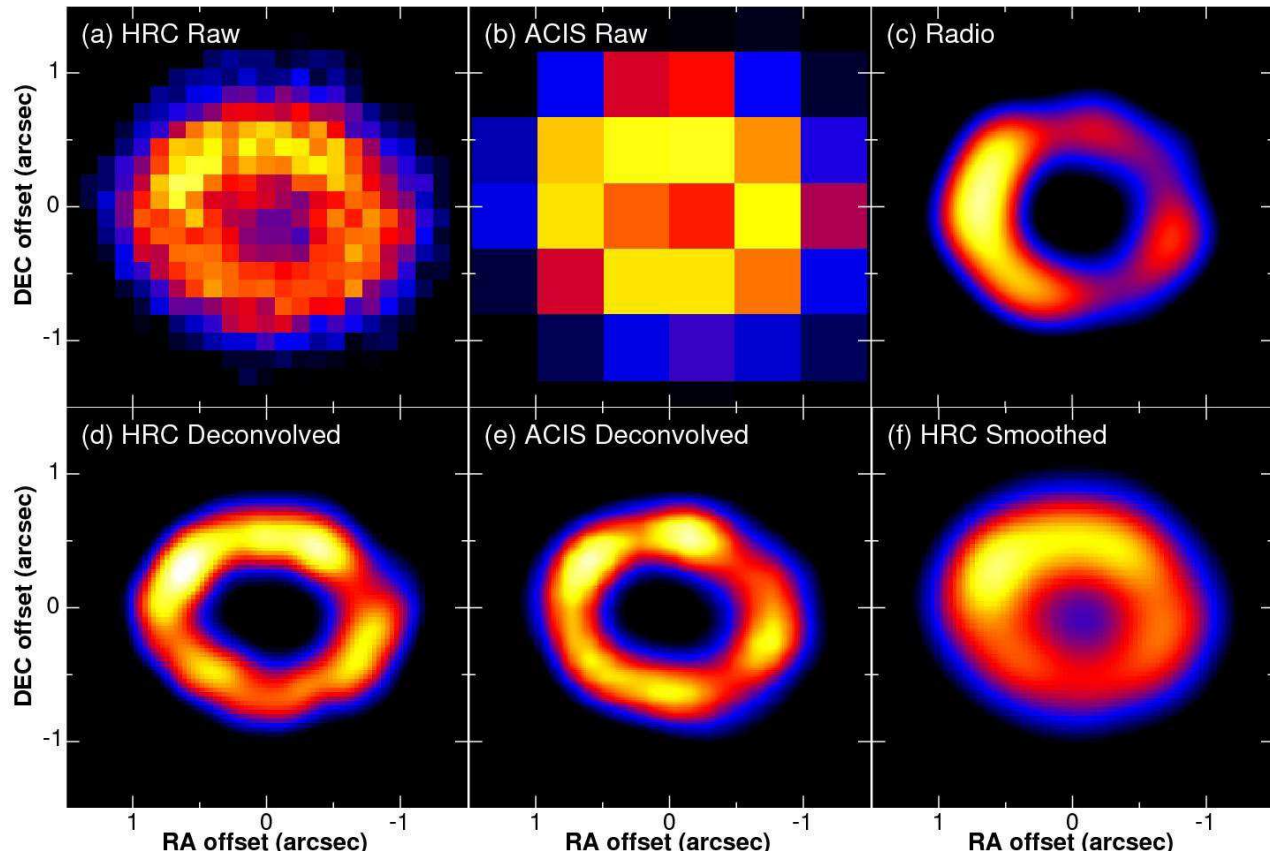


FIG. 1.— (a) Raw HRC data of SNR 1987A taken on 2008 Apr 28-29. The image was binned into the HRC detector pixel and centered at RA=05^h35^m28^s, Dec=−69°16′11.2″ (J2000). (b) Raw ACIS data taken on 2008 Jan 9. The image is in 0.3-8 keV energy range and was binned into the ACIS detector pixel. (c) Super-resolved radio image at 9 GHz taken by ATCA on 2008 Apr 23 (Ng et al. 2008). (d) Deconvolved HRC image using the dataset shown in panel (a). (e) Deconvolved ACIS image using the dataset shown in panel (b), in 0.3-8 keV energy range (Racusin et al. 2009). (f) HRC data in panel (a) smoothed to 0.4″ to match the resolution of the radio image in panel (c). All panels are on the same spatial scale.

2. OBSERVATION AND DATA REDUCTION

Our *Chandra* observations were carried out on 2008 Apr 28-29 (day 7736 since the SN explosion) using the HRC-I detector with a total exposure of 46 ks (ObsIDs 9085 and 9851). All the data reduction was carried out using CIAO 4.1⁶ with CALDB 4.1.1. In addition to standard data processing, we applied a screening algorithm (Murray et al. 2000) to reject the ‘bad events’ including non-X-ray background and mislocated events, thus improving the data quality and boosting the signal-to-noise ratio. There were no strong background flares during the exposure; hence all data were included in the analysis.

3. SPATIAL ANALYSIS AND RESULTS

The HRC image of SNR 1987A is shown in Figure 1a. This reveals a ring-like morphology for the remnant with a subluminescent region (a ‘hole’) at the center. The X-ray emission peaks in the northeast, and the north rim is generally brighter than the south. A comparison to the raw ACIS image at a similar epoch (2008 Jan 9) is shown in Figure 1b. The HRC image resolves, for the first time, the remnant structure with direct X-ray imaging, and reveals the central hole unambiguously. The entire remnant has $(3.0 \pm 0.02) \times 10^4$ cts in the full energy range (0.08-10 keV) of the HRC and the background is negli-

ble ($\sim 0.1\%$), implying a count rate of 0.66 ± 0.01 cts s^{−1}.

To further improve the resolution of the HRC image, we applied a similar deconvolution process as used by Burrows et al. (2000). The data were binned to a quarter of the detector pixel in each dimension, then deconvolved using the Lucy-Richardson algorithm (Lucy 1974) with a ChaRT/MARX⁷-simulated PSF at 1 keV, where both the source spectrum and the detector response peak.⁸ The resulting image after 30 iterations was smoothed to 0.2″ resolution and is shown in Figure 1d. As a comparison, we also showed in Figure 1e the deconvolution ACIS image from Racusin et al. (2009). In both images, the remnant exhibits a similar annular structure with sharp edges, and has semi-major and semi-minor axes of 0.8″ and 0.6″, respectively. There are some very minor difference in the extent of the bright regions between the two images, but the brightness variation is mostly continuous and smooth around the ring, and there is no obvious point source at the remnant center.

Figure 1c shows the super-resolved radio image of SNR 1987A at 9 GHz, taken by the ATCA at a similar epoch (2008 Apr 23; Ng et al. 2008). To obtain a direct comparison between the radio and X-ray images, we have regridded and smoothed the HRC data to the same resolution of 0.4″ FWHM, and the resulting image is shown

⁶ <http://cxc.harvard.edu/ciao/>

⁷ <http://cxc.harvard.edu/chart/>

⁸ <http://cxc.harvard.edu/proposer/POG/html/chap4.html>

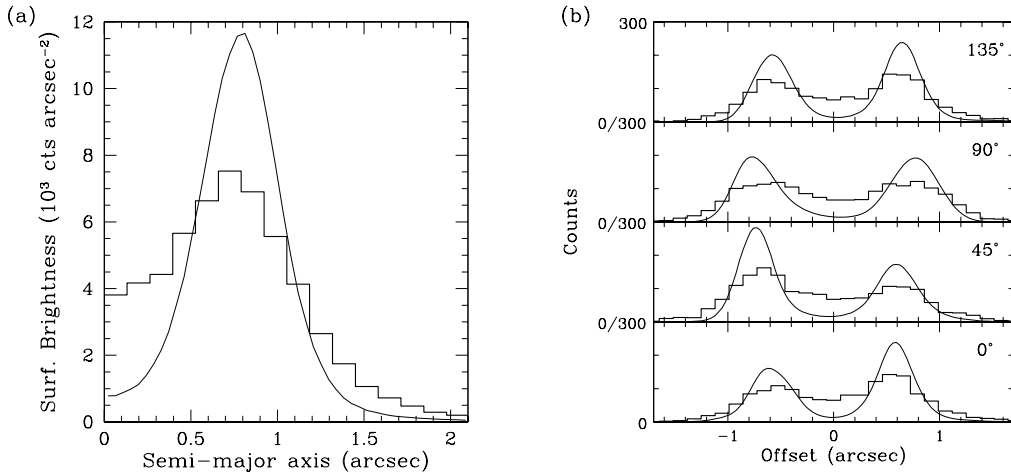


FIG. 2.— (a) Surface brightness profiles of SNR 1987A extracted from elliptical annulus regions (see text). (b) Slices through the remnant at different position angles (north through east). The offset is radial from the center and is positive toward north and/or west. In both plots, the raw and deconvolved HRC images are shown by the histograms and lines, respectively.

in Figure 1f. The radio shell consists of two main lobes: a bright one in the east and a fainter one in southwest; it has a similar size as the X-ray ring and both emissions peak in the east. Also, there is some hint of an X-ray counterpart for the southwestern radio lobe. However, except these similarities, the radio and X-ray emissions exhibit substantially different morphologies. While the former is mainly contributed by the eastern lobe, the latter is brightest along the north rim, and neither the overall bilateral pattern nor the strong east-west asymmetry in the radio image are observed in the HRC data.

We extracted surface brightness profiles for both raw and deconvolved HRC images using elliptical annulus regions with aspect ratios fixed by the system’s orientation (43.4° to the line of sight; Pun 2007), and the results are plotted in Figure 2a. The X-ray emission is very faint at the remnant center and peaks at about $0.8''$ radius with relatively sharp boundaries. The profile of the deconvolved image indicates a width of FWHM $0.5''$ for the ring, but we note that the actual width is likely smaller, since the deconvolved image has been smoothed. Figure 2b shows slices through the remnant along different position angles, illustrating a high degree of symmetry along the east-west direction. We found that counts in the eastern and western halves differ only by $5\% \pm 3\%$. In contrast, the north-south asymmetry is more significant ($25\% \pm 7\%$). It is partly due to the light travel time effect: the rapid brightening of the remnant makes the north rim, which is currently 1.5 light year closer to the Earth than the south rim, appear brighter. Based on the ACIS lightcurve, we estimated that this effect could result in at most 15% count difference between the northern and southern halves. However, it is not enough to account for the observed value; therefore, we conclude that the rest is intrinsic.

Motivated by the images, we have carried out detailed spatial modeling to capture the characteristic scales of the SNR. Simple models were generated in 3D, corrected for light travel time effects and projected onto the image plane according to the viewing geometry. The resulting images were then convolved with the PSF and fitted to the raw HRC data shown in Figure 1a using the procedure described by Ng & Romani (2008) with Gehrels

(1986) χ^2 statistic. Since we are mostly interested in the global geometry, we followed Ng et al. (2008) to account for the overall asymmetry using a linear brightness gradient with arbitrary position angle in the equatorial plane. It is worth noting that as compared to the recent ACIS study (Racusin et al. 2009), our fitting procedure involves no resampling or deconvolution processes that may degrade the data or introduce artifacts in the images. Therefore, it can provide robust measurements.

We have tried fitting various models, including a simple ring, an equatorial belt torus (see Ng et al. 2008), and a ring plus a shell. The best-fit parameters are listed in Table 1 with the corresponding images shown in Figure 3. Note that the formal reduced χ^2 values for the fits are likely underestimated, since the number of independent pixels in the image we are fitting is much larger than the source area. Better estimates of the reduced χ^2 values could be made using the source area of ~ 500 pixels. As shown in the table, this gives more reasonable results. The uncertainties quoted in Table 1 are statistical errors with 90% confidence level, estimated from Monte Carlo simulations (Ng & Romani 2008). We also followed their procedure to quantify systematic errors due to features not captured by the simple models, such as small-scale brightness fluctuations around the ring. This suggests a systematic uncertainty of $\sim 3\%$ for the radius. As indicated in Table 1, different fits give similar radii of $\sim 0.8''$, consistent with the plot in Fig. 2a. We found that a thin ring fits poorly to the data, but varying the ring’s thickness significantly improves the result. Our thick ring model is essentially same as the simple torus used in the ACIS study of Racusin et al. (2009), and the radius and thickness we obtained are in good agreement with their results. Our equatorial belt torus model offers a better fit than a ring, and suggests a half-opening angle $\sim 26^\circ$, slightly smaller than that of the radio shell (Ng et al. 2008; Potter et al. 2009). However, the characteristic two-lobe structure of the equatorial torus does not match the data (Fig. 3b). In terms of the statistics, our best model is given by a thin shell plus a thin ring. As shown in Figs. 3c & 3e, this model captures the overall remnant morphology well and successfully reproduces the observed ellipticity. The fit suggests 18%

TABLE 1
BEST-FIT SPATIAL MODELS TO 2008 APR 28-29 *Chandra* HRC IMAGE OF SNR 1987A

Model	Ring radius (")	Shell radius (")	Thickness (")	χ^2	dof ^a	χ^2_{ν} ^b
Thin ring	0.83 ± 0.01	...	0.04^c	1218	4090	2.4
Thick ring	0.75 ± 0.02	...	0.56 ± 0.08	942	4089	1.9
Torus ^d	...	0.82 ± 0.02	0.39 ± 0.02	884	4088	1.8
Ring+shell ^e	0.82 ± 0.03	0.94 ± 0.05	0.05^c	709	4088	1.4

NOTE. — The uncertainties quoted are statistical errors at 90% confidence level.

^a The formal number of degrees of freedom (dof) depends on the image size we are fitting, and they are likely overestimated (see text).

^b The reduced χ^2 values, χ^2_{ν} , are estimated with dof=500, as we argued in the text.

^c Fixed at 5% of the corresponding radii during the fit.

^d The best-fit torus has a half-opening angle $26^\circ \pm 3^\circ$.

^e The fit suggest 18% more counts in the ring than the shell component.

more counts in the ring component than the shell. While it is tempting to associate the latter with faster shocks at a higher latitude, the physical scenario is likely to be more complicated and the parameters in the fits could be highly degenerate. Further observations are needed to confirm if a two-component spatial model is required.

Similar to Ng et al. (2008), we added a point source at the center of the best-fit model to estimate the flux limit from any possible central object. We adjusted the point source flux and re-fit the model until the χ^2 value exceeded a certain level. This gives a detection limit 0.010 cts s^{-1} at 99% confidence level over the energy range 0.08-10 keV. For a $R^\infty = 13 \text{ km}$ radius⁹ neutron star 51.4 kpc away with a foreground neutral hydrogen column density $N_{\text{H}} = 1.3 \times 10^{21} \text{ cm}^{-2}$ (Zhekov et al. 2009), the flux limit corresponds to a surface temperature $T^\infty = 2.50 \text{ MK}$, or a bolometric luminosity $L_{\text{bol}}^\infty = 4.7 \times 10^{34} \text{ ergs s}^{-1}$. More physical estimates using neutron star atmosphere models (e.g. Zavlin et al. 1996) suggest similar values. If the radiation from the central source is nonthermal with a typical powerlaw index $\Gamma = 1.5$, then the limit converts to a luminosity of $7.0 \times 10^{34} \text{ ergs s}^{-1}$ in 2-10 keV energy range. To have a fair comparison with previously published values, we followed Park et al. (2004) to ignore the statistical fluctuations of the underlying remnant, and repeated the above exercise. This gives a 90% confidence level detection limit $3.3 \times 10^{34} \text{ ergs s}^{-1}$ in the 2-10 keV range, slightly higher than the ACIS limit of $1.5 \times 10^{34} \text{ ergs s}^{-1}$ (Park et al. 2004), likely due to the brightening of the remnant, but more stringent than the *XMM-Newton* limit $5 \times 10^{34} \text{ ergs s}^{-1}$ obtained from spectral analysis (Shtykovskiy et al. 2005).

4. DISCUSSION

4.1. X-ray Morphology of SNR 1987A

The HRC observations of SNR 1987A have provided a direct X-ray image that confirms the remnant structure as suggested by previous ACIS observations using the deconvolution technique (Racusin et al. 2009, and references therein). As the image shows, the entire X-ray ring has been lit up, and its size and ellipticity are in good accord with the optical inner ring. This gives direct evidence that the blast wave has already encountered

the dense CSM all around the ring and is now interacting with the main body of the ring. The deconvolved HRC and ACIS images are nearly identical, except for some very minor differences in the brightness distribution, which could be attributed to the different energy response of the instruments. Zhekov et al. (2009) reported a strong energy dependence of the east-west asymmetry in the ACIS data. The eastern half is dominated by hotter plasmas behind fast shocks, therefore it is brighter at higher energies. Conversely, the western half has cooler plasmas, slower shocks and is brighter at lower energies. These two contributions could possibly cancel out in the HRC image, resulting in the high degree of symmetry observed along the east-west direction. We are unable to verify this because the HRC data do not possess any spectral information. As the shocks further propagate and decelerate in the dense CSM, we expect the degree of symmetry to vary in future observations.

The poor spatial correlation between the soft X-ray and radio morphologies suggests that they may originate from different physical processes. While the X-rays trace the SN blast wave, the radio emission is believed to originate between the forward and reverse shocks (Manchester et al. 2005; Ng et al. 2008). Given the young age of SNR 1987A, both shocks should have similar radii (e.g. Truelove & McKee 1999), hence, one would expect the X-ray and radio shells to have a comparable size. A direct comparison between the HRC and radio images in Figure 1 seems to support this picture. Nonetheless, previously reported radii for the X-ray shell have always been 10-15% smaller than for the radio shell (Ng et al. 2008; Racusin et al. 2009). The discrepancy could be due to different measuring techniques (Gaensler et al. 2007; Racusin et al. 2009), or due to systematic errors in the measurements. A better way to compare the sizes is from the outer edge of the shells. This can avoid complication by the inner ring or projection effects. After accounting for the shell's thickness, our best-fit model of the HRC image has an outer radius of $0.96''$. Similar values are obtained from other models (see Table 1), and it also seems consistent with the ACIS study (Racusin et al. 2009). All these indicate that our estimate is robust, thus, we conclude that the X-ray shell has an outer radius of $0.96'' \pm 0.05'' \pm 0.03''$, with the uncertainties corresponding to statistical (90% confidence) and systematic errors, respectively. This is very similar to the outer radius $0.92'' \pm 0.06''$ of the radio

⁹ This is the redshifted value as observed at infinity, same for the temperature and luminosity below.

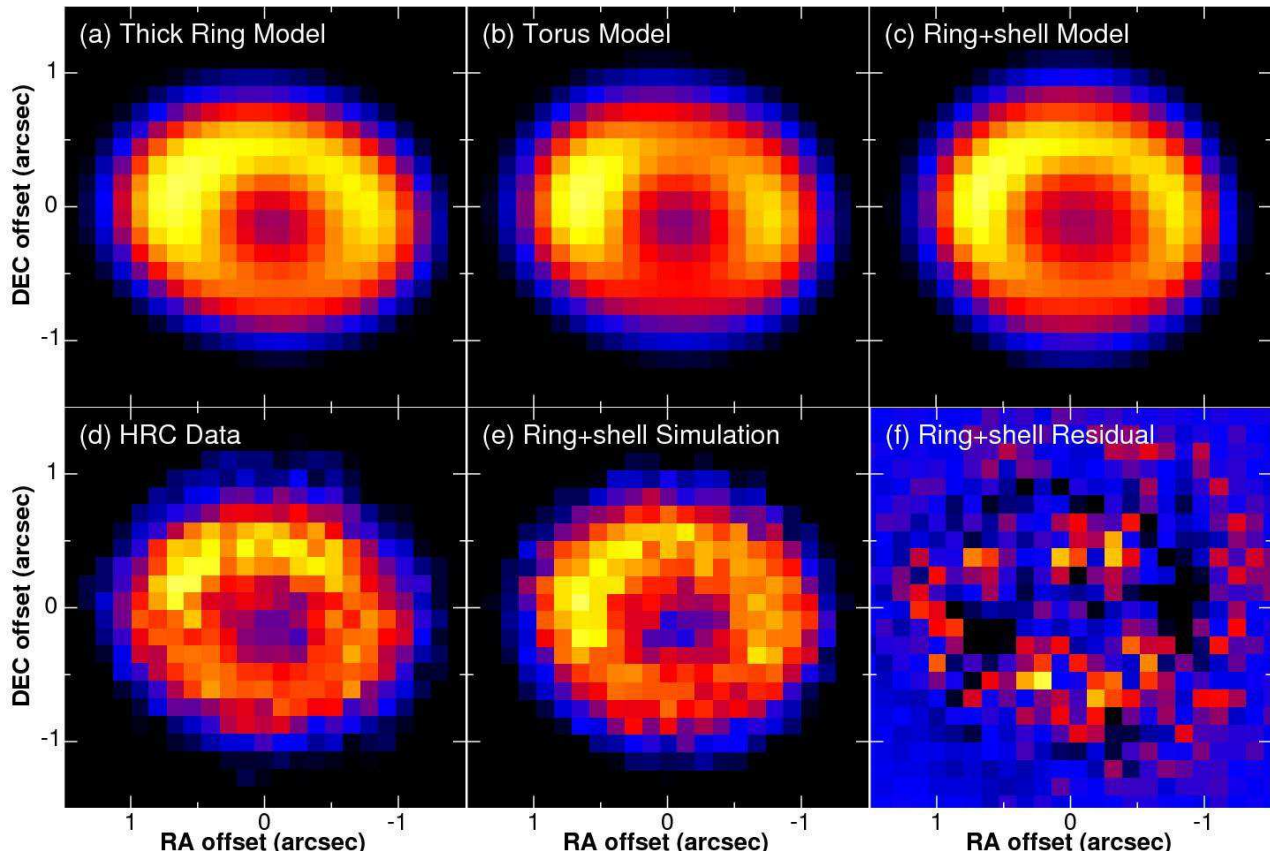


FIG. 3.— Best-fit spatial models for the HRC image of SNR 1987A: (a) a thick ring, (b) a torus, (c) a thin ring plus a thin shell. All images are convolved with the instrument PSF. (d) The HRC data, same as Fig. 3a. (e) MARX simulation of the best-fit ring plus shell model from (c). (f) Difference image between panels (d) and (c), showing the residuals of the fit. All panels except (f) are on the same color range.

shell (Potter et al. 2009), thus confirming the physical picture discussed above. Although these values appear to be slightly larger than the optical inner ring of radius $0.81''$ - $0.86''$ (Burrows et al. 1995; Plait et al. 1995), they unlikely represent the radius of the transmitted shock inside the dense CSM, since which should have a very slow propagation speed according to some hydrodynamic simulations (e.g. Dwarkadas 2007). Therefore, we believe that our results could correspond to the projected size of fast shocks traveling in a lower density environment at higher latitudes.

4.2. X-ray Limit on a Central Source

In the absence of fast cooling mechanisms, standard theories suggest a bolometric luminosity $L_{\text{bol}}^{\infty} \geq 5.0 \times 10^{34} \text{ erg s}^{-1}$ (corresponding to a surface temperature $T^{\infty} \approx 2.54 \text{ MK}$) for a 21-year-old neutron star (Yakovlev & Pethick 2004; Shternin & Yakovlev 2008). Our flux limit rejects any unobscured neutron stars hotter than this at 99% confidence. Graves et al. (2005) argued that a neutron star obscured by dust is unlikely, since the IR flux is consistent with the radioactive decay of ^{44}Ti in the ejecta and no other energy source is required. The same conclusion also holds for the recent IR observations (Bouchet et al. 2006). On the other hand, for a neutron star with short thermal relaxation time due to superfluidity, quark matter, or anomalously high thermal conductivity of the crust, the thermal emission from the surface could have already been too low to detect

at an age of 21 (Shternin & Yakovlev 2008; Chan et al. 2009).

X-ray emission from a young pulsar is often dominated by nonthermal radiation from the magnetosphere and from the surrounding pulsar wind nebula (PWN). The nonthermal flux limit we derived rules out energetic pulsars such as the Crab or PSR B0540-69, but a fainter pulsar/PWN system similar to 3C 58 would still escape detection (see Kargaltsev & Pavlov 2008). These authors also gave a general correlation between nonthermal luminosity and spin-down power \dot{E} of young pulsars, which places a conservative limit $\dot{E} < 3 \times 10^{37} \text{ erg s}^{-1}$ for the unseen pulsar in SNR 1987A. Based on the non-detection, Ögelman & Alpar (2004) argued that the pulsar, if it exists, should have either a very strong or very weak magnetic field. While the former case would put the star into the magnetar regime, our detection limit is incompatible with the X-ray luminosities of nearly all known magnetars, even in quiescence (Woods & Thompson 2006; Mereghetti 2008). For the weakly magnetized neutron star case, one candidate is a central compact object (CCO), which is a soft X-ray source found inside a SNR, and could possibly be a neutron star born with a weak magnetic field (see review by Gotthelf & Halpern 2008). It has been proposed that SNR 1987A may harbor a CCO (e.g. Manchester 2007; Halpern et al. 2007); however, the current observations do not provide any useful constraints on this scenario, unless CCOs have similar cooling properties as discussed

above. Finally, we note that Graves et al. (2005) considered different accretion models and used the UV flux limit to rule out spherical accretion and a slim disk, where the disk thickness is non-negligible. They also placed stringent constraints on thin-disk models. Although it is beyond the scope of this paper to reproduce their modeling, given the similar order of our X-ray limit, we believe that our results unlikely improve their constraints substantially.

5. CONCLUSION

We have presented a detailed analysis of *Chandra* HRC observations of supernova remnant 1987A. The remnant has a similar size as the optical inner ring, and its morphology is statistically best-fitted by a thin ring plus a thin shell. This provides direct evidence that the dense

inner ring of circumstellar medium has been overtaken the supernova blast wave. Our spatial modeling also indicates a similar size between the X-ray- and radio-emitting regions, confirming the picture that the supernova forward and reverse shocks are closely located. The X-ray flux limit on any possible central source rejects a young neutron star, unless it has some fast cooling mechanisms or is obscured by a small accretion disk.

We thank Svetozar Zhekov and Dima Yakovlev for useful discussions. C.-Y.N. and B.M.G. acknowledge the support of the Australian Research Council through grant FF0561298. This work was supported in part through NASA Contract NAS 5-38248. *Facilities:* CXO (HRC)

REFERENCES

- Bouchet, P., et al. 2006, *ApJ*, 650, 212
 Burrows, C. J., et al. 1995, *ApJ*, 452, 680
 Burrows, D. N., et al. 2000, *ApJ*, 543, L149
 Chan, T. C., Cheng, K. S., Harko, T., Lau, H. K., Lin, L. M., Suen, W. M., & Tian, X. L. 2009, *ApJ*, 695, 732
 Dwarkadas, V. V. 2007, in *AIP Conf. Proc.*, Vol. 937, *Supernova 1987A: 20 Years After: Supernovae and Gamma-Ray Bursters*, ed. S. Immler, K. Weiler, & R. McCray (New York: AIP), 120
 Gaensler, B. M., Staveley-Smith, L., Manchester, R. N., Kesteven, M. J., Ball, L., & Tzioumis, A. K. 2007, in *AIP Conf. Proc.*, Vol. 937, *Supernova 1987A: 20 Years After: Supernovae and Gamma-Ray Bursters*, ed. S. Immler, K. Weiler, & R. McCray (New York: AIP), 86
 Gehrels, N. 1986, *ApJ*, 303, 336
 Gotthelf, E. V., & Halpern, J. P. 2008, in *AIP Conf. Proc.*, Vol. 983, *40 Years of Pulsars: Millisecond Pulsars, Magnetars and More*, ed. C. Bassa, Z. Wang, A. Cumming, & V. M. Kaspi (New York: AIP), 320
 Graves, G. J. M., et al. 2005, *ApJ*, 629, 944
 Halpern, J. P., Gotthelf, E. V., Camilo, F., & Seward, F. D. 2007, *ApJ*, 665, 1304
 Kargaltsev, O., & Pavlov, G. G. 2008, in *AIP Conf. Proc.*, Vol. 983, *40 Years of Pulsars: Millisecond Pulsars, Magnetars and More*, ed. C. Bassa, Z. Wang, A. Cumming, & V. M. Kaspi (New York: AIP), 171
 Lucy, L. B. 1974, *AJ*, 79, 745
 Manchester, R. N. 2007, in *AIP Conf. Proc.*, Vol. 937, *Supernova 1987A: 20 Years After: Supernovae and Gamma-Ray Bursters*, ed. S. Immler, K. Weiler, & R. McCray (New York: AIP), 134
 Manchester, R. N., Gaensler, B. M., Staveley-Smith, L., Kesteven, M. J., & Tzioumis, A. K. 2005, *ApJ*, 628, L131
 Mereghetti, S. 2008, *A&A Rev.*, 15, 225
 Morris, T., & Podsiadlowski, P. 2007, *Science*, 315, 1103
 Murray, S. S., et al. 2000, in *Proc. SPIE*, Vol. 4140, *X-Ray and Gamma-Ray Instrumentation for Astronomy XI*, ed. K. A. Flanagan & O. H. Siegmund, 144
 Ng, C.-Y., Gaensler, B. M., Staveley-Smith, L., Manchester, R. N., Kesteven, M. J., Ball, L., & Tzioumis, A. K. 2008, *ApJ*, 684, 481
 Ng, C.-Y., & Romani, R. W. 2008, *ApJ*, 673, 411
 Ögelman, H., & Alpar, M. A. 2004, *ApJ*, 603, L33
 Park, S., Zhekov, S. A., Burrows, D. N., Garmire, G. P., & McCray, R. 2004, *ApJ*, 610, 275
 Park, S., Zhekov, S. A., Burrows, D. N., Garmire, G. P., Racusin, J. L., & McCray, R. 2006, *ApJ*, 646, 1001
 Park, S., Zhekov, S. A., Burrows, D. N., & McCray, R. 2005, *ApJ*, 634, L73
 Plait, P. C., Lundqvist, P., Chevalier, R. A., & Kirshner, R. P. 1995, *ApJ*, 439, 730
 Potter, T. M., et al. 2009, *ApJ*, 705, 261
 Pun, C. S. J. 2007, in *American Institute of Physics Conference Series*, Vol. 937, *Supernova 1987A: 20 Years After: Supernovae and Gamma-Ray Bursters*, ed. S. Immler, K. Weiler, & R. McCray (New York: AIP), 171
 Racusin, J. L., Park, S., Zhekov, S., Burrows, D. N., Garmire, G. P., & McCray, R. 2009, *ApJ*, 703, 1752
 Shternin, P. S., & Yakovlev, D. G. 2008, *Astronomy Letters*, 34, 675
 Shtykovskiy, P. E., Lutovinov, A. A., Gilfanov, M. R., & Sunyaev, R. A. 2005, *Astronomy Letters*, 31, 258
 Truelove, J. K., & McKee, C. F. 1999, *ApJS*, 120, 299
 Tsunemi, H., Mori, K., Miyata, E., Baluta, C., Burrows, D. N., Garmire, G. P., & Chartas, G. 2001, *ApJ*, 554, 496
 Woods, P. M., & Thompson, C. 2006, in *Compact stellar X-ray sources*, ed. W. H. G. Lewin & M. van der Klis (Cambridge, UK: Cambridge University Press), 547
 Yakovlev, D. G., & Pethick, C. J. 2004, *ARA&A*, 42, 169
 Zavlin, V. E., Pavlov, G. G., & Shibanov, Y. A. 1996, *A&A*, 315, 141
 Zhekov, S. A., McCray, R., Dewey, D., Canizares, C. R., Borkowski, K. J., Burrows, D. N., & Park, S. 2009, *ApJ*, 692, 1190